Faraday Discussions
Cite this: DOI: 10.1039/d4fd00209a

ROYAL SOCIETY OF CHEMISTRY

PAPER
View Article Online
View Journal

Published on 23 January 2025. Downloaded by Westlake University on 5/14/2025 2:08:32 PM.

Programming two-component peptide self-assembly by tuning the hydrophobic linker†

Sangshuang Li, Huayang Liu, Yu Fang, Yaoting Li, Laicheng Zhou, Dinghao Chen, Juan Liang and Huaimin Wang *

Received 25th December 2024, Accepted 20th January 2025
DOI: 10.1039/d4fd00209a

Molecular self-assembly enables the formation of intricate networks through non-covalent interactions, serving as a key strategy for constructing structures ranging from molecules to macroscopic forms. While zero-dimensional and one-dimensional nanostructures have been widely achieved, two-dimensional nanostrip structures present unique advantages in biomedical and other applications due to their high surface area and potential for functionalization. However, their efficient design and precise regulation remain challenging. This study systematically explores how different hydrophobic amino acid linkers impact the microscopic morphology in two-component co-assembly systems with strong electrostatic interactions. The introduction of the AA linker resulted in distinctive 2D nanostrips, which stacked to form bilayer sheets, whereas VV, LL, and NleNle linkers formed one-dimensional fibers. In contrast, GG and PP linkers did not produce stable aggregates. Our findings highlight the role of intermolecular interactions in the development of 2D assemblies, providing new insights into the design and application of 2D materials.

1 Introduction

Molecular self-assembly has emerged as a key strategy for constructing complex nanostructures through the modulation of non-covalent intermolecular interactions, including hydrogen bonding, hydrophobic interactions, and electrostatic forces.[1–7] This dynamic approach mimics natural molecular interactions, offering a powerful strategy to build structures ranging from individual molecules to macroscopic forms. While zero-dimensional and one-dimensional nanostructures have been extensively studied in peptide and biomolecule self-assembly,[8–17] two-dimensional lamellar structures—such as nanostrips and

Department of Chemistry, Westlake University, Institute of Natural Sciences, Westlake Institute for Advanced Study, 18 Shilongshan Road, Hangzhou 310024, Zhejiang Province, China. E-mail: wanghuaimin@westlake.edu.cn

† Electronic supplementary information (ESI) available. See DOI: https://doi.org/10.1039/d4fd00209a

Published on 23 January 2025. Downloaded by Westlake University on 5/14/2025 2:08:32 PM.

nanosheets, exhibit significant potential in biomedicine, nanomaterials, and energy storage due to their unique stability, anisotropic properties, and high surface area for functionalization.[18–24] However, the efficient design and precise regulation of 2D lamellar structures remain major challenges in current molecular self-assembly research.

One major difficulty lies in achieving the right balance between self-assembly kinetics and thermodynamic stability.[20,21,25] The formation of stable 2D structures, such as nanostrips and nanosheets, requires careful modulation of intermolecular interactions, including hydrogen bonding, hydrophobic interactions, and electrostatic forces. In this context, multicomponent co-assembled systems offer unique opportunities to generate more intricate structural motifs and dynamically tuneable pathways by strategically combining different noncovalent interactions.[26–30] However, the complexity of multicomponent co-assembled systems can lead to unpredictable outcomes, as variations in the composition and arrangement of molecules can significantly influence the assembly process.[31] This complexity makes it challenging to consistently produce desired structural features and functionalities.

In previous studies, our group has successfully constructed multicomponent co-assembled systems exhibiting liquid-crystal states predominantly through the electrostatic interactions of positively and negatively charged peptides.[32] These interactions, along with other noncovalent forces such as π–π stacking interactions and hydrogen bonding, led to the formation of one-dimensional nanofibers and highlighted the importance of intermolecular forces in guiding self-assembly dynamics. However, while this peptide backbone—stabilized primarily by electrostatic interactions and π–π stacking interactions—enabled precise molecular alignment, it also confined the resulting architectures largely to one-dimensional forms. To move beyond one-dimensional nanofibers toward two-dimensional, lamellar-type structures, it is necessary to introduce additional noncovalent interactions that can complement and modulate these existing driving forces. Hydrophobic interactions, another fundamental class of noncovalent forces, are well-known for their capacity to construct higher-order structures.[33] Previous studies have demonstrated that hydrophobic linkers with different alkyl side chains markedly affect the properties of the assemblies.[34] Therefore, we hypothesized that incorporating hydrophobic linkers in the middle of a short peptide into our tetrapeptide systems would likely generate 2D nanostructures, which could provide new insights into the mechanisms and provide valuable guidance for the design of complex higher-order structures.

We designed and introduced a series of hydrophobic dipeptide linkers with varying hydrophobicity and side-chain structures (including GG, AA, LL, VV, and NleNle) into positively and negatively charged peptide co-assembly systems. We systematically investigated their effects on the microscopic morphology and macroscopic properties of the peptide assemblies. The results demonstrated that the type of hydrophobic linker significantly influenced both the assembly behavior and the final structural properties of the system. Notably, the AA linkers formed nanostrip structures that stacked layer-by-layer into regular three-dimensional bilayer sheet-like structures. Atomic force microscopy (AFM) revealed that the sheet thickness of the AA system is about 6 nm, resulting from the stacking of two ~3 nm nanostrip layers. In contrast, the VV, LL, and NleNle linkers primarily formed one-dimensional fibrous structures, while the GG and

 This journal is © The Royal Society of Chemistry 2025

Published on 23 January 2025. Downloaded by Westlake University on 5/14/2025 2:08:32 PM.

PP linkers failed to create stable aggregates due to their hydrophobicity or side-chain configurations. Fourier-transform infrared (FTIR) spectroscopy revealed that the AA linker system formed a β-sheet secondary structure, and wide-angle X-ray scattering (WAXS) indicated a highly ordered molecular structure.

2 Results and discussion

2.1 Molecular design and synthesis

Molecular self-assembly has emerged as a powerful strategy for constructing nanostructures, finding extensive applications in nanomaterials and biomedicine due to its capability to create complex and ordered structures through non-covalent interactions (such as hydrogen bonding, hydrophobic interactions, and electrostatic interactions).[1] For instance, Gazit and coworkers have extensively studied the self-assembly behavior of dipeptides like phenylalanine–phenylalanine (FF), establishing a significant foundation for the investigation of short-peptide self-assembly.[12]

Recently, our lab successfully developed a multicomponent system exhibiting a liquid-crystal-like structure, driven by electrostatic interactions, which facilitates the formation of one-dimensional nanofiber structures. This work, alongside other studies, has demonstrated that subtle tuning of non-covalent interactions within a two-component self-assembly system is an effective strategy for controlling high-order structural formation.[26–30,32] In this context, we incorporated tuneable hydrophobic linkers into the previously investigated co-assembly peptide scaffolds Ac-FKFK-NH_2 and Ac-FEFE-NH_2 to explore their self-assembly properties and evaluate the influence of these hydrophobic linkers on the microscopic morphology of the resulting assemblies (Table 1). Our objective was to investigate the potential of this strategy for the preparation of functional two-dimensional sheet-like materials.

In our design (Fig. 1), we selected hydrophobic linkers with varying degrees of hydrophobicity and distinct side-chain structures (namely, GG, AA, LL, VV, PP, and NleNle) to connect two identical binding domains. By modulating these linkers, we aimed to control the assembly behavior and final morphology of the peptides. To minimize unwanted intermolecular interactions, we restricted

Table 1 Peptide sequences and characteristics of their mixtures used in this study

Sample	Peptide sequence	Aggregation behavior	Morphology
[AA] mixture	Ac-FEAAFE-NH_2, Ac-FKAAFK-NH_2	Hydrogel	Nanostrip
[LL] mixture	Ac-FELLFE-NH_2, Ac-FKLLFK-NH_2	Hydrogel	Fiber
[VV] mixture	Ac-FEVVFE-NH_2, Ac-FKVVFK-NH_2	Hydrogel	Fiber
[NleNle] mixture	Ac-FENleNleFE-NH_2, Ac-FKNleNleFK-NH_2	No gelation (turbid solution + precipitates)	Fiber
[GG] mixture	Ac-FEGGFE-NH_2, Ac-FKGGFK-NH_2	No aggregation	—
[PP] mixture	Ac-FEPPFE-NH_2, Ac-FKPPFK-NH_2	No aggregation	—

Published on 23 January 2025. Downloaded by Westlake University on 5/14/2025 2:08:32 PM.

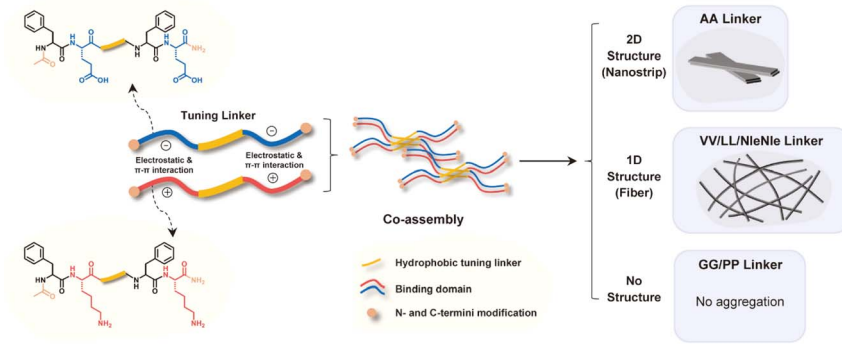

Fig. 1 Illustration of the self-assembly of programmed two-component peptides by tuning the hydrophobic linker.

electrostatic interactions among the peptide molecules to occur between the side chains, achieved through acetylation and amidation modifications at the N- and C-termini. This approach reduces additional ionization, enhances the hydrophobicity of the peptides, and allows us to focus on how the tuning of peptide side chains influences self-assembly behavior.

All peptides were synthesized *via* standard Fmoc solid-phase peptide synthesis (SPPS) using rink amide resin, ensuring the formation of the C-terminal amide structure, and avoiding additional ionization *via* N-terminal acetylation. Peptide purity and structure during synthesis were confirmed using proton nuclear magnetic resonance (^{1}H NMR) (Fig. S8–S19†) and liquid chromatography-mass spectrometry (LC-MS) (Fig. S20†), with all peptides achieving a purity of at least 95%.

2.2 Macroscopic behaviour and properties

2.2.1 Critical aggregation concentration. The aggregation propensity of positively and negatively charged peptide monomers, as well as their equimolar mixed systems, was assessed by determining the critical aggregation concentration (CAC), a key parameter for understanding the self-assembly behaviour of peptide systems in solution.[35] We prepared a 10 mM solution of a single peptide at pH 7.4 and then mixed it in equal volume with another peptide to create a two-component system.

The experimental results indicated that the CAC values of the two-component systems were generally lower than those of the corresponding single peptides (Fig. S1†), suggesting that the combination of positive and negative charges enhances intermolecular aggregation. Notably, the [VV] mixture, [AA] mixture, and [LL] mixture exhibited lower CAC values, indicating a stronger tendency for aggregation due to enhanced hydrophobic interactions in solution. In contrast, the CAC values for the GG and PP linker systems could not be determined within the tested range, highlighting their weaker intermolecular aggregation capabilities (Fig. 2). These findings underscore the crucial role of hydrophobic linkers in promoting peptide aggregation.

2.2.2 Gelation behaviour. The gelation kinetics and behaviour of different linker systems were examined by observing the time required for hydrogel

 This journal is © The Royal Society of Chemistry 2025

Published on 23 January 2025. Downloaded by Westlake University on 5/14/2025 2:08:32 PM.

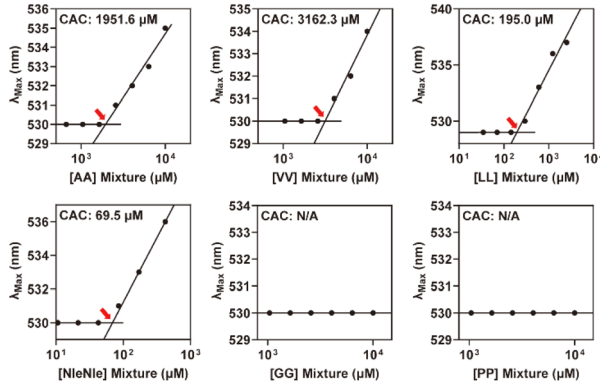

Fig. 2 CAC results of the two-component systems in an aqueous solution (pH = 7.4) after 24 hours of incubation.

formation (Fig. 3). The hydrogelation time of different linker systems varied significantly. The [AA] mixture exhibited a slow gelation process, taking approximately 10 days to achieve a stable hydrogel. In contrast, the [VV] mixture and [LL] mixture formed stable hydrogels much more quickly, in 5 hours and 2 days, respectively, demonstrating their superior gel-forming abilities and shorter assembly times. The [NleNle] mixture, however, failed to establish a stable water-encapsulating gel network due to excessive aggregation, resulting in a turbid liquid phase.

The [GG] mixture and [PP] mixture did not form gels under the same conditions and remained clear liquids, indicating their weaker gel-forming capabilities. For the [GG] and [PP] mixtures, these observations may be attributed to the distinct structural features of the two linkers. Specifically, the GG linker, lacking side chains, is minimally hydrophobic and exhibits substantial conformational

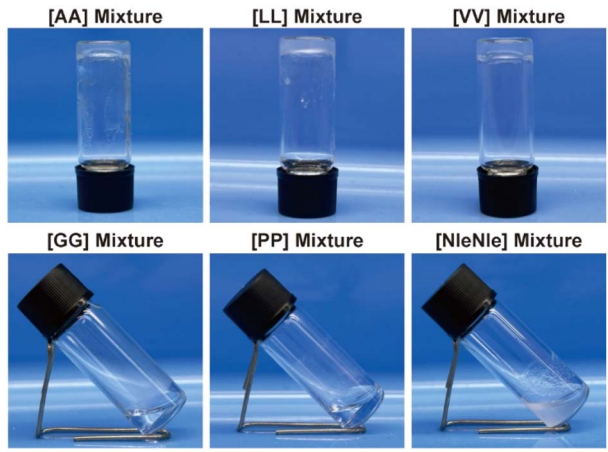

Fig. 3 Optical images of the two-component systems in an aqueous solution (pH = 7.4) at a concentration of 10.0 mM. The [AA] mixture formed a stable hydrogel in 10 days, [LL] in 2 days, and [VV] in 5 hours.

Published on 23 January 2025. Downloaded by Westlake University on 5/14/2025 2:08:32 PM.

flexibility, conditions that hinder the establishment of effective aggregation and prevent the formation of stable structures.[36] In the case of the PP linker, the absence of hydrogen-bond donors and the rigidity imposed by its cyclic side chain severely limit conformational adaptability and molecular packing.[37] As a result, neither the [GG] nor the [PP] mixture forms assemblies or stable hydrogels.

2.2.3 Mechanical properties. To evaluate the mechanical properties of hydrogels formed by different linker systems, we conducted rheological analyses on the three hydrogel-forming mixtures. Strain-scanning tests were performed first (Fig. S2†). The results indicated that the energy storage modulus (G') exceeded the loss modulus (G'') across all systems within the strain range of 0.01% to 5.0%, with only weak dependence of G' and G'' on strain. This suggests a stable hydrogel formation. However, both G' and G'' began to decline when the strain exceeded approximately 10%, indicating that the hydrogel network experiences damage at larger strains. The intersection points of the G' and G'' curves occurred at 11.8% for the [LL] mixture, 9.8% for the [VV] mixture, and 5.9% for the [AA] mixture. This behavior may be attributed to the structural stability of the network formed by different morphologies.

For the frequency-sweep test, we selected a strain of 0.1% within the linear response range of 0.01% to 1% (Fig. 4). The frequency-scan results showed that the G' of all three hydrogels remains higher than their G'', resulting in a loss factor (tan δ) that stays below 1 throughout the 0.01–100 Hz frequency range (Fig. S3†). Consequently, these hybrid hydrogels display predominantly elastic behavior,

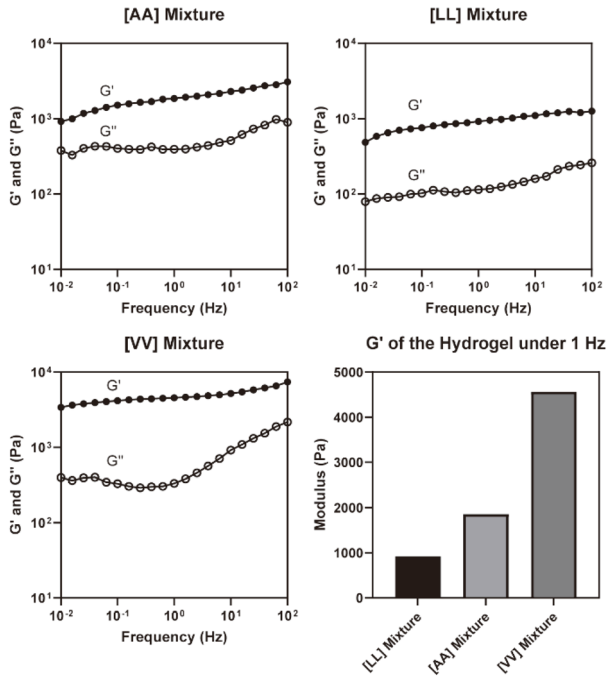

Fig. 4 Frequency sweep of the hydrogel (10.0 mM) formed by the [AA] mixture, [LL] mixture and [VV] mixture after stabilization in aqueous solution (pH 7.4) under the strain of 0.1%, and the G' at 1 Hz.

 This journal is © The Royal Society of Chemistry 2025

Published on 23 January 2025. Downloaded by Westlake University on 5/14/2025 2:08:32 PM.

indicating a gel-like characteristic structure. In the [LL] and [AA] mixture systems, both the energy storage modulus and loss modulus remained relatively constant with increasing frequency. This stability indicates that these hydrogels are highly resistant to external shear and can maintain their structural integrity under stress. In contrast, the [VV] mixture exhibited a more pronounced change in G'', particularly at higher frequencies, suggesting greater susceptibility to external shear and increased energy dissipation under high-frequency conditions.

Comparing the G' values of the hydrogels at 1 Hz (Fig. 4), our analysis revealed distinct trends in rigidity, stability, and resistance to deformation among the different linker systems: [VV] mixture > [AA] mixture > [LL] mixture. Specifically, the [VV] mixture displayed the strongest mechanical stability and resistance to deformation, while the [AA] mixture demonstrated moderate stability and toughness, and the [LL] mixture exhibited the weakest mechanical properties.

2.3 Characterization of peptide assembly

2.3.1 Morphological observations. We conducted transmission electron microscopy (TEM) to characterize the single peptides and the mixed systems of positively and negatively charged peptides, aiming to observe their microscopic morphology and explore the impact of different hydrophobic linkers on assembly morphology (Fig. S4† and Fig. 5).

The TEM images reveal that the AA linker system forms a distinct two-dimensional nanostrip structure with a width ranging from 200 to 300 nm. Compared to the two AA-linker single peptides, which lack a discernible morphology, the mixture exhibits a well-defined sheet-like arrangement. This observation indicates that the AA linker significantly promotes peptide self-assembly, stabilizing the formation of a regular two-dimensional structure. This effect may stem from the extended gelation time, which allows for a more gradual and organized assembly process, ultimately leading to a more complex and well-organized nanostructure. In contrast, the [VV] mixture, [LL] mixture, and [NleNle] mixture primarily yield one-dimensional nanofiber structures. The [VV] mixture features thick, entangled nanofibers with diameters around 15–40 nm,

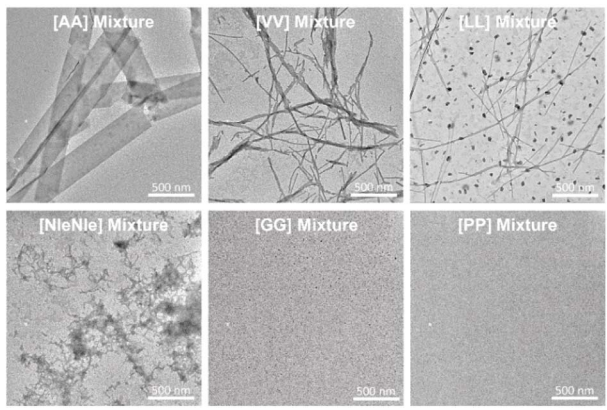

Fig. 5 TEM images of the two-component systems (10.0 mM) in an aqueous solution (pH 7.4).

Published on 23 January 2025. Downloaded by Westlake University on 5/14/2025 2:08:32 PM.

while the [LL] mixture consists of elongated nanofibers measuring 25–40 nm, with some fibers accompanied by nanoparticles. The [NleNle] mixture, however, produces shorter and thinner nanofibers that aggregate into clusters. The [GG] mixture and [PP] mixtures, on the other hand, do not exhibit distinct morphological features in the TEM images, suggesting a weak ability to form nanostructures under the tested conditions.

2.3.2 Characterization of 2D nanostructures. To assess the thickness of the two-dimensional structures formed by the [AA] mixture, we measured the height of the assembled nanostructures using atomic force microscopy (AFM). The AFM images (Fig. S5†) confirm the lamellar structures observed in the TEM analysis. We selected a representative assembly for detailed measurement and recorded the height measurements at three different locations. The results indicate that the assembly consists of two overlapping nanostrips, each measuring approximately 3 nm in height, resulting in a total thickness of 6 nm for the bilayer nanostrip (Fig. 6).

Additionally, a larger field of view characterization (Fig. S5†) revealed that while some scattered assembled monoliths were present, the majority exhibited aggregated stacking. Most of the assembled monoliths measured 6 nm in thickness, further supporting the conclusion that the assemblies predominantly consist of bilayer two-dimensional structures.

2.3.3 Secondary-structure analysis. To further characterize the structural properties of the [AA] mixture assemblies and investigate the nature of their assembly, we analyzed their secondary structures using Fourier-transform infrared (FTIR) spectroscopy (Fig. 7). The FTIR spectra were recorded in the amide I region (1600–1700 cm^{-1}), which is particularly sensitive to the secondary structure of peptides.[38] The spectrum of the assembled system displayed characteristic absorption peaks corresponding to different secondary structures. Notably, the [AA] mixture exhibits a strong absorption peak at approximately 1621 cm^{-1}, indicating a predominantly β-sheet-like structure.

We also conducted FTIR characterization of the single peptides and other mixed systems, revealing that the spectral features varied among different linker systems (Fig. S6†). This variation suggests that the choice of hydrophobic linker has a significant impact on the secondary structure of peptide assemblies.

2.3.4 Molecular packing analysis. To further investigate the stacking pattern of the [AA] mixture assemblies, we characterized their *d*-spacing using wide-angle

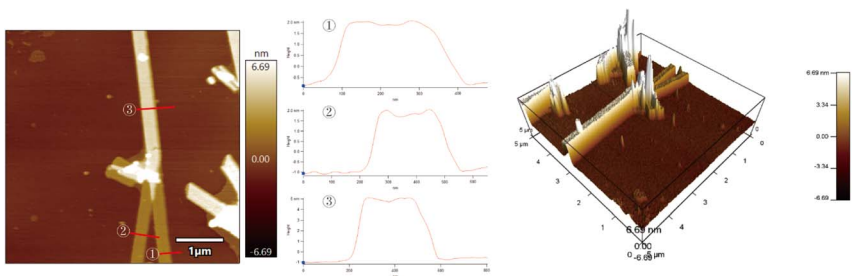

Fig. 6 AFM image of the [AA] mixture (10.0 mM) in an aqueous solution (pH 7.4) and height measurement of a typical assembly at three locations, (1), (2) and (3).

 This journal is © The Royal Society of Chemistry 2025

Published on 23 January 2025. Downloaded by Westlake University on 5/14/2025 2:08:32 PM.

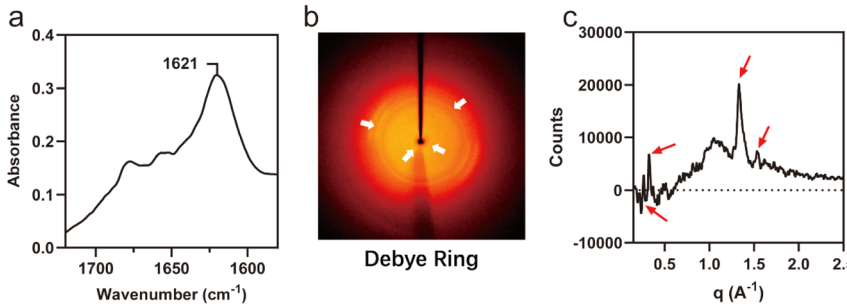

Fig. 7 Secondary structure and molecular packing analysis of the [AA] mixture (10.0 mM) in an aqueous solution (pH 7.4): (a) FTIR spectrum, (b) WAXS Debye rings, and (c) integrated WAXS spectrum.

X-ray scattering (WAXS) (Fig. 7).[39] The WAXS analysis revealed a distinct periodic structure in the diffraction pattern, with calculated *d*-spacing values of 23.65 Å, 19.46 Å, 4.72 Å, and 4.10 Å, reflecting different molecular arrangements within the assembly. Notably, the *d*-spacing value of 4.72 Å corresponds to the –N–H···O=C– hydrogen bonding characteristic of the β-sheet structure,[40,41] which aligns with the β-sheet-like structure observed in the FTIR analysis. The larger *d*-spacing values of 23.65 Å and 19.46 Å likely reflect the periodic arrangement of molecules in the lateral direction, indicating the presence of a layered structure. Specifically, the 19.46 Å spacing may represent both the thickness of the monolayer and the interlayer spacing. Subtracting the 4.72 Å spacing of the β-sheet layer from the 19.46 Å yields 14.74 Å, which approximates half the thickness of the monomolecular layer and is consistent with the approximately 3 nm layer thickness measured *via* atomic force microscopy (AFM). This suggests that the internal arrangement of the assemblies may involve the stacking of two molecular layers to form a thin layer about 3 nm thick, which then stacks to create a larger 6 nm structure. The characteristic peak at 6 nm is not observed in the WAXS data, which may be attributed to the limitations of the WAXS measurement range, which typically captures a maximum spacing of about 5 nm.

Additionally, we performed WAXS measurements on other hydrogel-forming systems (Fig. S7†), revealing distinct patterns of molecular stacking across different hydrophobic linker systems. Analysis of the WAXS data for the [AA] mixture, [VV] mixture, and [LL] mixture revealed significant differences in molecular arrangement and structural periodicity. Conversely, the stacking patterns of the [VV] and [LL] mixtures displayed less pronounced periodicity, likely related to the structural differences in their linker side chains, further highlighting the influence of hydrophobic linkers on the molecular stacking modes of the assemblies.

3 Experimental

3.1 Materials

All reagents and chemicals used in this study were of analytical grade and employed without further purification. Fmoc-protected amino acids and HBTU (2-(1*H*-benzotriazole-1-yl)-1,1,3,3-tetramethyluronium hexafluorophosphate) were

Published on 23 January 2025. Downloaded by Westlake University on 5/14/2025 2:08:32 PM.

sourced from GL Biochem Ltd. (China). Piperidine, diethyl ether, and acetic anhydride were obtained from Sinopharm Chemical Reagent Co., Ltd. (China). *N*,*N*-Diisopropylethylamine (DIPEA), rhodamine 6G, and triisopropylsilane (TIS) were purchased from Aladdin Biochemical Technology Co., Ltd. (Shanghai, China). Uranyl acetate was procured from RXSV CHEM Co., Ltd. (China). Rink amide resin was supplied by Hecheng Science & Technology Co., Ltd. (China), while *N*,*N*-dimethylformamide (DMF) was obtained from J&K Scientific Co., Ltd. (China). Trifluoroacetic acid (TFA) was purchased from Energy Chemical Co., Ltd. (China).

3.2 Synthesis of peptides

Peptides were synthesized *via* solid-phase peptide synthesis (SPPS) using Fmoc chemistry on rink amide resin. The Fmoc deprotection step was performed using 20% piperidine in *N*,*N*-dimethylformamide (DMF). After synthesis, the N-terminus of the peptides was acetylated using acetic anhydride. The peptides were cleaved from the resin using a TFA/TIS/water (95%/2.5%/2.5%) cocktail for 2 hours. The crude peptides were precipitated in cold diethyl ether, and the purity was determined using high-performance liquid chromatography (HPLC). The peptides were further characterized *via* LC-MS (Agilent, U.S.A.) and ^{1}H NMR spectroscopy (Bruker BioSpin, Switzerland).

3.3 Preparation of co-assembly systems

To prepare the co-assembly systems, peptides were dissolved in water at a concentration of 10.0 mM, and the pH was adjusted to 7.4 using 0.1 M NaOH. Equal volumes of positively charged peptide solution and negatively charged peptide solution were mixed, followed by vortexing to allow co-assembly into mixed-component systems.

3.4 Critical aggregation concentration (CAC)

The CAC assay was performed by mixing rhodamine 6G (working concentration: 5 μM) with peptide solutions, followed by incubation at room temperature for 24 hours.[42,43] The maximum absorption wavelength (λ_{max}) of rhodamine 6G was then measured using a microplate reader (Varioskan LUX, Thermo Fisher, USA) to evaluate the CAC.

3.5 Rheological analysis

Rheological measurements were performed using a TA-Waters ARES-G2 rheometer (USA) to analyze the mechanical properties of the hydrogels. The co-assembly mixture was transferred into a 5 mL syringe with the top removed and sealed with Parafilm.[44] The samples were then incubated until the hydrogels reached a stable state, defined as no further observable changes in physical properties such as gelation or flow behavior. Specifically, the [LL] and [VV] mixtures were incubated for 6 days, while the [AA] mixture required 12 days to reach stability. The hydrogel was subsequently loaded onto the rheometer, utilizing an upper plate with a 25 mm diameter and a gap height of 0.40 mm under controlled conditions at 25 °C. The strain sweep was conducted from 0.01% to 100% strain at a constant frequency of 1 Hz. The frequency sweep was conducted from 0.01 Hz to 100 Hz at a fixed strain amplitude of 0.1%.

 This journal is © The Royal Society of Chemistry 2025

Published on 23 January 2025. Downloaded by Westlake University on 5/14/2025 2:08:32 PM.

3.6 Transmission electron microscopy (TEM)

All samples were incubated in water for 15 days before being used for TEM analysis. The samples (4 μL) were placed onto 200 mesh carbon-coated copper grids and incubated for 1 minute. Excess solution was removed with filter paper. The samples were stained with a 2% (w/v) uranyl acetate solution (4 μL) for 1 minute, and images were acquired using a Talos L120C TEM (Thermo Fisher, Netherlands) at 120 kV.

3.7 Atomic force microscopy (AFM)

AFM was conducted using a Cypher VRS Environmental AFM (Oxford Instruments, USA) to analyze the surface morphology of the [AA] mixture incubated in water for 15 days. A 50 μL sample (10.0 mM) was deposited onto a mica substrate and dried using a strong stream of nitrogen gas. AFM imaging was performed in tapping mode under ambient conditions at room temperature.

3.8 Fourier-transform infrared (FTIR) spectroscopy

FTIR spectra of the hydrogels were recorded using a Nicolet iS50 spectrometer (Thermo Scientific, USA) equipped with an attenuated total reflectance (ATR) accessory. The samples were incubated in water for 15 days to reach assembly stability, then freeze-dried. The resulting solid powders were analyzed directly using FTIR. Spectra were recorded in the range of 4000–400 cm^{-1}.

3.9 Wide-angle X-ray scattering (WAXS)

The molecular packing and structural arrangement of the hydrogel samples were analyzed *via* wide-angle X-ray scattering (WAXS) using the D8 VENTURE METALJET Single Crystal X-ray Diffractometer (SC-XRD) with Gα radiation ($\lambda = 1.34138$ Å). The *d*-spacing values were determined from the diffraction patterns, where $q = (4\pi)\sin(\theta)/\lambda = 2\pi/d$; 2θ is the scattering angle, λ is the wavelength of X-ray source, and d is the real-space distance.[39] The measurements were performed after the hydrogels reached stability. Specifically, the mixtures of [LL] and [VV] were incubated in water for 6 days, while [AA] was incubated for 12 days.

4 Conclusions

In this study, we explored the self-assembly properties of peptide systems using various hydrophobic linkers, with a particular focus on the [AA] mixture. Our findings demonstrate that the choice of linker significantly influences the morphology, structure, and mechanical properties of peptide assemblies. The formation of two-dimensional nanostrip structures, characterized by a β-sheet-like arrangement, highlights the role of hydrophobic interactions and molecular packing in achieving stable assemblies. The use of techniques such as TEM, AFM, FTIR, and WAXS provided comprehensive insights into the structural characteristics and assembly mechanisms of these systems.

The distinct periodicity observed in the [AA] mixture suggests a highly ordered molecular structure, which is advantageous for potential applications in functional materials, including drug delivery systems, tissue engineering, and nanotechnology. The comparative analysis with other mixtures, such as [VV] and [LL],

Published on 23 January 2025. Downloaded by Westlake University on 5/14/2025 2:08:32 PM.

emphasizes the importance of hydrophobic linkers in modulating assembly behavior and structural integrity.

Looking ahead, further research could explore the incorporation of additional functional groups or the optimization of linker designs to enhance the stability and responsiveness of these peptide assemblies. Investigating the dynamic behavior of these systems under varying environmental conditions—such as pH, temperature, and ionic strength—could provide deeper insights into their practical applications. Additionally, expanding the scope to include more complex multicomponent systems may yield novel materials with tailored properties for specific biomedical and industrial applications.

Data availability

The data supporting this article have been included as part of the ESI.†

Author contributions

The manuscript was written through contributions of all authors. All authors have given approval to the final version of the manuscript.

Conflicts of interest

The authors declare no competing financial interest.

Acknowledgements

This project was supported by the National Key Research and Development Program of China (2022YFB3808300), and the National Natural Science Foundation of China (82272145).

Notes and references

1 A. J. Savyasachi, O. Kotova, S. Shanmugaraju, S. J. Bradberry, G. M. Ó'Máille and T. Gunnlaugsson, *Chem*, 2017, **3**, 764–811.
2 J. Zhan, Y. Cai, S. He, L. Wang and Z. Yang, *Angew. Chem., Int. Ed.*, 2018, **57**, 1813–1816.
3 Y. Ding, D. Zheng, L. Xie, X. Zhang, Z. Zhang, L. Wang, Z.-W. Hu and Z. Yang, *J. Am. Chem. Soc.*, 2023, **145**, 4366–4371.
4 Z. Feng, H. Wang, X. Chen and B. Xu, *J. Am. Chem. Soc.*, 2017, **139**, 15377–15384.
5 A. G. Cheetham, R. W. Chakroun, W. Ma and H. Cui, *Chem. Soc. Rev.*, 2017, **46**, 6638–6663.
6 L. A. Haines, K. Rajagopal, B. Ozbas, D. A. Salick, D. J. Pochan and J. P. Schneider, *J. Am. Chem. Soc.*, 2005, **127**, 17025–17029.
7 M. Kumar, N. L. Ing, V. Narang, N. K. Wijerathne, A. I. Hochbaum and R. V. Ulijn, *Nat. Chem.*, 2018, **10**, 696–703.
8 L. Liu, K. Xu, H. Wang, P. K. J. Tan, W. Fan, S. S. Venkatraman, L. Li and Y.-Y. Yang, *Nat. Nanotechnol.*, 2009, **4**, 457–463.

 This journal is © The Royal Society of Chemistry 2025

Published on 23 January 2025. Downloaded by Westlake University on 5/14/2025 2:08:32 PM.

9 H. Yokoi, T. Kinoshita and S. Zhang, *Proc. Natl. Acad. Sci. U. S. A.*, 2005, **102**, 8414–8419.
10 J. D. Hartgerink, E. Beniash and S. I. Stupp, *Science*, 2001, **294**, 1684–1688.
11 A. R. Hirst, S. Roy, M. Arora, A. K. Das, N. Hodson, P. Murray, S. Marshall, N. Javid, J. Sefcik, J. Boekhoven, J. H. v. Esch, S. Santabarbara, N. T. Hunt and R. V. Ulijn, *Nat. Chem.*, 2010, **2**, 1089–1094.
12 M. Reches and E. Gazit, *Science*, 2003, **300**, 625–627.
13 P.-P. He, X.-D. Li, L. Wang and H. Wang, *Acc. Chem. Res.*, 2019, **52**, 367–378.
14 H. Wang, Y. Song, W. Wang, N. Chen, B. Hu, X. Liu, Z. Zhang and Z. Yu, *J. Am. Chem. Soc.*, 2024, **146**, 330–341.
15 R. Zheng, J. Yang, M. Mamuti, D. Y. Hou, H. W. An, Y. Zhao and H. Wang, *Angew. Chem.*, 2021, **133**, 7888–7898.
16 X. Yan, P. Zhu and J. Li, *Chem. Soc. Rev.*, 2010, **39**, 1877–1890.
17 R. Chang, C. Yuan, P. Zhou, R. Xing and X. Yan, *Acc. Chem. Res.*, 2024, **57**, 289–301.
18 C.-A. Palma and P. Samorì, *Nat. Chem.*, 2011, **3**, 431–436.
19 J. Sakamoto, J. v. Heijst, O. Lukin and A. D. Schlüter, *Angew. Chem., Int. Ed.*, 2009, **48**, 1030–1069.
20 J. W. Colson and W. R. Dichtel, *Nat. Chem.*, 2013, **5**, 453–465.
21 L. Liu, L. H. Klausen and M. Dong, *Nano Today*, 2018, **23**, 40–58.
22 W.-H. Zhang, B.-J. Jiang and P. Yang, *Chin. Chem. Lett.*, 2016, **27**, 1339–1344.
23 E. R. Draper and D. J. Adams, *Chem. Soc. Rev.*, 2018, **47**, 3395–3405.
24 H. Shigemitsu, T. Fujisaku, W. Tanaka, R. Kubota, S. Minami, K. Urayama and I. Hamachi, *Nat. Nanotechnol.*, 2018, **13**, 165–172.
25 J. Wang, K. Liu, R. Xing and X. Yan, *Chem. Soc. Rev.*, 2016, **45**, 5589–5604.
26 X.-D. Xu, C.-S. Chen, B. Lu, S.-X. Cheng, X.-Z. Zhang and R.-X. Zhuo, *J. Phys. Chem. B*, 2010, **114**, 2365–2372.
27 I. W. Hamley, A. Dehsorkhi and V. Castelletto, *Langmuir*, 2013, **29**, 5050–5059.
28 H. Frisch, J. P. Unsleber, D. Lüdeker, M. Peterlechner, G. Brunklaus, M. Waller and P. Besenius, *Angew. Chem., Int. Ed.*, 2013, **52**, 10097–10101.
29 J. R. Wester, J. A. Lewis, R. Freeman, H. Sai, L. C. Palmer, S. E. Henrich and S. I. Stupp, *J. Am. Chem. Soc.*, 2020, **142**, 12216–12225.
30 S. Panja, A. Seddon and D. J. Adams, *Chem. Sci.*, 2021, **12**, 11197–11203.
31 L. Li, R. Sun and R. Zheng, *Mater. Des.*, 2021, **197**, 109209.
32 B. Wu, S. Zhao, X. Yang, L. Zhou, Y. Ma, H. Zhang, W. Li and H. Wang, *ACS Nano*, 2022, **16**, 4126–4138.
33 S. F. Tan, S. Raj, G. Bisht, H. V. Annadata, C. A. Nijhuis, P. Král and U. Mirsaidov, *Adv. Mater.*, 2018, **30**, 1707077.
34 P. C. Lyu, J. C. Sherman, A. Chen and N. R. Kallenbach, *Proc. Natl. Acad. Sci. U. S. A.*, 1991, **88**, 5317–5320.
35 S. Y. Fung, C. Keyes, J. Duhamel and P. Chen, *Biophys. J.*, 2003, **85**, 537–548.
36 H. Dong, M. Sharma, H.-X. Zhou and T. A. Cross, *Biochemistry*, 2012, **51**, 4779–4789.
37 P. Chakrabarti and S. Chakrabarti, *J. Mol. Biol.*, 1998, **284**, 867–873.
38 R. Arunkumar, C. J. Drummond and T. L. Greaves, *Front. Chem.*, 2019, **7**, 74.
39 P. Müller-Buschbaum, *Adv. Mater.*, 2014, **26**, 7692–7709.
40 S. Tassler, D. Pawlowska, C. Janich, J. Giselbrecht, S. Drescher, A. Langner, C. Wölk and G. Brezesinski, *Phys. Chem. Chem. Phys.*, 2018, **20**, 17393–17405.
41 A. Datar, K. Balakrishnan and L. Zang, *Chem. Commun.*, 2013, **49**, 6894–6896.

42 H. S. Courtney, W. A. Simpson and E. H. Beachey, *Infect. Immun.*, 1986, **51**, 414–418.
43 J. Wang, L. Hu, H. Zhang, Y. Fang, T. Wang and H. Wang, *Adv. Mater.*, 2022, **34**, 2104704.
44 E. R. Draper, E. G. B. Eden, T. O. McDonald and D. J. Adams, *Nat. Chem.*, 2015, **7**, 848–852.

Published on 23 January 2025. Downloaded by Westlake University on 5/14/2025 2:08:32 PM.

 This journal is © The Royal Society of Chemistry 2025